Modelling, Simulation and Flight Test of a Model Predictive Controlled Multirotor with Heavy Slung Load

Notter S. [*] **Heckmann A.** [*] **Mcfadyen A.** [**] **Gonzalez F.** [**]

[*] *Institute of Flight Mechanics and Control, University of Stuttgart, Germany (e-mail: stefan.notter@ifr.uni-stuttgart.de)*
[**] *Australian Research Centre for Aerospace Automation, Queensland University of Technology, Brisbane, Australia, (e-mail: aaron.mcfadyen@qut.edu.au, felipe.gonzalez@qut.edu.au)*

Abstract: A controller for stable flight and precise tracking of a multirotor unmanned aerial vehicle (UAV) carrying a heavy slung load is presented within this paper. A novel mathematical model for the multi-body system is derived. Based on that model, a Model Predictive Control (MPC) scheme is designed and applied to the system. Stability and tracking ability are demonstrated through numerical simulation. The performance of the system using the MPC strategy is compared to a linear-quadratic regulator (LQR) control approach. The simulation results are then verified by real flight tests, whereby the MPC is applied to a real multirotor UAV with a heavy slung load. The system is capable of actively damping load oscillations whilst simultaneously tracking a reference trajectory.

Keywords: Unmanned Aerial Vehicle, Multirotor, Slung Load, Model Predictive Control

1. INTRODUCTION

Due to their special flight characteristics, multirotor UAVs are well suited to deliver loads even in a range of operational environments. Highly autonomous platforms may also prove to be a cost effective alternative to existing delivery methods. However, autonomous landing in complex and unknown terrain can become hazardous. Carrying suspended loads might be a suitable approach to delivery that can overcome such issues. Using suspended loads could also benefit other other applications as well, particularly in the agriculture, plant biosecurity and fire fighting sectors. For example, close proximity measurements could be taken by sensors placed underneath a multirotor flying at a safe height above the plants. Their is also the possibility of collecting gas and volatile organic compound sensor data uninfluenced by rotor downwash. The flight control strategies presented within this paper could be extended to manned operations such as those used to combat fires.

Regardless of the application or platform, it is important to ensure stable flight characteristics and precise positioning of both the vehicle and the load. The stability and tracking performance of the system is highly affected by the dynamics of the slung load. Aggressive flight manoeuvres that result in large load oscillations can cause instability. The Model Predictive Control (MPC) approach directly takes the dynamics of the coupled system into account. Constraints can be set on both the state variables and the control input. Thus, the risk of undesirable or dangerous flight conditions is minimised. Solving an optimal control problem (OCP) subject to the predicted system behavior in the future, the MPC approach also offers superior tracking of predefined, four-dimensional trajectories.

Some research has focused on controller design for manned helicopters carrying an external load. A simple anti-swing controller for a conventional helicopter with a slung load is presented by Omar [2009]. Optimal control strategies for a helicopter slung load system are designed and simulated in Oktay and Sultan [2013]. A cascaded control algorithm for a quadrotor UAV with a cable suspended load is developed by Sreenath et al. [2013]. Simulation results for two-dimensional movement of a coupled system controlled by several control algorithms including MPC approaches are presented by Trachte et al. [2014].

The contributions and the structuring of this work are as follows: A novel, three-dimensional model describing the dynamics of a coupled system including a multirotor UAV with heavy slung load is presented in section 2. The model takes the coupling into account without making simplifications in that regard. Even so, a closed-form representation of the system dynamics is obtained. Based on this model, an MPC strategy is derived. Both the basic principle of Model Predictive Control and the specific implementation are set out in section 3. For the given implementation, simulation results indicate the MPC scheme's superior ability for tracking a predefined, time-dependent reference in comparison to a system using an LQR control approach. The simulation results are shown in section 4. Feasibility and performance of the control strategy are demonstrated through flights tests using a real indoor quadrotor setup. Both the experimental setup and the flight test results are presented in section 5.

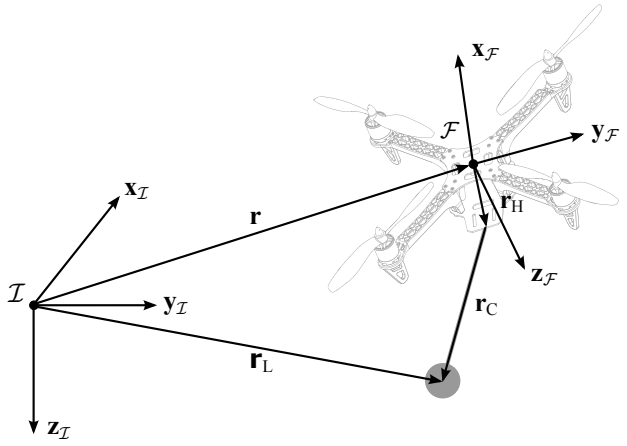

Fig. 1. Relevant frames of references and position vectors for a high-level control approach

2. MODELLING OF THE SYSTEM DYNAMICS

To implement an MPC controller, a model of the system dynamics is required. The model is used to predict the future states of the system, and should represent the true system dynamics to ensure a useful control solution will be obtained. Additionally, the model should be kept simple to reduce the computational cost. The dynamics in this case refer to the coupled system including the multirotor, suspended load and underlying low-level controller. Experimental results for a small quadrotor prove that the low-level controlled vehicle dynamics are sufficiently fast (cf. Lupashin et al. [2014]). The low-level control therefore allows for quasi-instantaneous control of the vehicle attitude rates, so the low-level controller dynamics can be neglected. The multirotor and load dynamics are derived in the following section, and are based on those presented by Hehn and D'Andrea [2011]. However, the model presented in this paper explicitly includes the loads reactive forces on the vehicle, and is therefore better suited for heavy loads.

2.1 Multirotor dynamics

The inertial frame of reference is denoted by $\mathcal{I} = \{\mathbf{x}_\mathcal{I}, \mathbf{y}_\mathcal{I}, \mathbf{z}_\mathcal{I}\}$, where $\mathbf{z}_\mathcal{I}$ is the unit vector parallel to the gravity vector. The body fixed frame of reference $\mathcal{F} = \{\mathbf{x}_\mathcal{F}, \mathbf{y}_\mathcal{F}, \mathbf{z}_\mathcal{F}\}$ is related to the inertial frame by the rotation matrix $\mathbf{R} : \mathcal{F} \to \mathcal{I}$. The inertial frame of reference and the body fixed frame of reference are illustrated in Fig. 1. The attitude vector is denoted by $\boldsymbol{\phi} = (\phi, \theta, \psi)$. The rotation matrix $\mathbf{R}$ as stated in equation (1) is defined by the transposed composition of sequential rotations about the yaw angle ψ, the pitch angle θ, and the roll angle ϕ.

The position vector pointing to the centre of gravity of the vehicle is denoted by $\mathbf{r} = (x, y, z)$. The vectors $\mathbf{v} = (u, v, w)$ and $\boldsymbol{\omega} = (p, q, r)$ are the linear and angular velocity vectors in the body fixed frame. The equations of motion of the multirotor can be expressed as

$$\dot{\mathbf{r}} = \mathbf{R}\mathbf{v}\,, \tag{2}$$

$$\dot{\mathbf{v}} = -\boldsymbol{\omega} \times \mathbf{v} + g\mathbf{R}^\mathrm{T}\mathbf{z}_\mathcal{I} + \frac{1}{m_F}\left(\mathbf{R}^\mathrm{T}\left(\mathbf{f}_H + \mathbf{f}_D\right) - f_T\mathbf{z}_\mathcal{F}\right)\,, \tag{3}$$

$$\dot{\boldsymbol{\phi}} = \mathbf{J}\boldsymbol{\omega}\,, \tag{4}$$

where g is the gravitational acceleration and m_F is the mass of the multirotor. The aerodynamic drag force of the vehicle is denoted by $\mathbf{f}_D$. The collective thrust f_T of the rotors is given by

$$f_T = \sum_{i=1}^{N_R} f_i\,, \tag{5}$$

where N_R is the number of rotors of the vehicle. As the aerodynamic drag force of the vehicle is small compared to the thrust of the multirotor, it is neglected hereafter. $\mathbf{f}_H$ is the force acting on the suspension point due to the load, which will be derived in the following subsection. The matrix $\mathbf{J}$ converts the rates of the Euler angles to the body system. It is given by:

$$\mathbf{J} = \frac{1}{\cos(\theta)}\begin{bmatrix} \cos(\theta) & \sin(\phi)\sin(\theta) & \cos(\phi)\sin(\theta) \\ 0 & \cos(\phi)\cos(\theta) & -\sin(\phi)\cos(\theta) \\ 0 & \sin(\phi) & \cos(\phi) \end{bmatrix} \tag{6}$$

Equation (3) is denoted with respect to the body fixed frame of reference in order to comply with flight mechanics convensions. All the other equations in this section are denoted with respect to the inertial frame of reference.

2.2 Load dynamics

The position vector of the load with respect to the inertial frame of reference is denoted by $\mathbf{r}_L = (x_L, y_L, z_L)$. $\mathbf{v}_L = (u_L, v_L, w_L)$ is the inertial velocity of the load denoted in inertial coordinates and $\boldsymbol{a}_L$ is the inertial acceleration of the load . The three-degrees-of-freedom equations of motion are given by:

$$\dot{\mathbf{r}}_L = \mathbf{v}_L\,, \tag{7}$$

$$\dot{\mathbf{v}}_L = \mathbf{a}_L\,. \tag{8}$$

The position vector of the load with respect to the suspension point $\mathbf{r}_C$ is given by

$$\mathbf{r}_C = \mathbf{r}_L - (\mathbf{r} + \mathbf{R}\mathbf{r}_H)\,, \tag{9}$$

where $\mathbf{r}_H$ denotes the displacement of the suspension point with respect to the center of gravity of the vehicle. The relevant position vectors for the model described in this

$$\mathbf{R} = \left(\underbrace{\begin{bmatrix} 1 & 0 & 0 \\ 0 & \cos(\phi) & \sin(\phi) \\ 0 & -\sin(\phi) & \cos(\phi) \end{bmatrix}}_{=\mathbf{R}_x(\phi)} \underbrace{\begin{bmatrix} \cos(\theta) & 0 & -\sin(\theta) \\ 0 & 1 & 0 \\ \sin(\theta) & 0 & \cos(\theta) \end{bmatrix}}_{=\mathbf{R}_y(\theta)} \underbrace{\begin{bmatrix} \cos(\psi) & \sin(\psi) & 0 \\ -\sin(\psi) & \cos(\psi) & 0 \\ 0 & 0 & 1 \end{bmatrix}}_{=\mathbf{R}_z(\psi)} \right)^T . \tag{1}$$

section are illustrated in Fig. 1. Friction in both the cord and the suspension point is neglected. The inertial acceleration of the load $\mathbf{a}_L$ is then derived by assuming equilibrium of moments about the suspension point such that

$$\mathbf{r}_C \times \mathbf{f}_H = 0\,, \tag{10}$$

where $\mathbf{f}_H$ describes the force acting on the multirotor due to the load:

$$\mathbf{f}_H = -m_L \mathbf{a}_L + m_L g \mathbf{z}_\mathcal{I} + \mathbf{f}_{D,L}\,. \tag{11}$$

The aerodynamic drag force of the load is denoted by $\mathbf{f}_{D,L}$:

$$\mathbf{f}_{D,L} = -\frac{1}{2} C_{D,L} \rho A_L \left\|\mathbf{v}_L\right\|_2 \mathbf{v}_L\,. \tag{12}$$

$C_{D,L}$ is the drag coefficient of the load referred to the relevant cross-section area of the load A_L. The density of the air is denoted by ρ. $\|\cdot\|_2$ refers to the Euclidean norm in $\mathbb{R}^3$. Evaluating equation (11) assures that only longitudinal force is transmitted by the cable.

Assuming the cable length l to be constant, a kinematic constraint is given by:

$$\left\|(\mathbf{r} + \mathbf{R}\mathbf{r}_H) - \mathbf{r}_L\right\|_2 = l\,. \tag{13}$$

Assuming the suspension point to be located near the centre of gravity of the vehicle ($\mathbf{r}_H \approx 0$), the z-component of the load position can easily be derived from equation (13)

$$z_L = z + \sqrt{l^2 - \Delta_x^2 - \Delta_y^2}\,, \tag{14}$$

where $\Delta_x = x - x_L$ and $\Delta_y = y - y_L$. Only the solution with $z_L > z$ is taken into account. Differentiating equation (13) twice

$$\underbrace{\dot{\Delta}_x \Delta_x + \dot{\Delta}_y \Delta_y}_{=:H} + \dot{\Delta}_z \Delta_z = 0\,, \tag{15}$$

$$\underbrace{\dot{\Delta}_x^2 + \ddot{\Delta}_x \Delta_x + \dot{\Delta}_y^2 + \ddot{\Delta}_y \Delta_y + \dot{\Delta}_z^2}_{=:G} + \ddot{\Delta}_z \Delta_z = 0\,, \tag{16}$$

the z-component of the velocity and acceleration can eventually be written as

$$\dot{z}_L = \frac{H}{\Delta_z} + \dot{z}\,, \tag{17}$$

$$\ddot{z}_L = \frac{G}{\Delta_z} + \ddot{z}\,, \tag{18}$$

where $\Delta_z = z - z_L$.

The state vector of the coupled system is therefore given by

$$\mathbf{x} = (\mathbf{r}, \mathbf{v}, \boldsymbol{\phi}, x_L, y_L, u_L, v_L)\,. \tag{19}$$

The input vector for high-level control is then given by:

$$\mathbf{u} = (\boldsymbol{\omega}, f_T)\,. \tag{20}$$

Equations (2) to (11) describe the coupled system dynamics for high-level control as a set of ordinary differential equations:

$$\mathbf{F}\left(\dot{\mathbf{x}}, \mathbf{x}, \mathbf{u}\right) = \mathbf{0}\,. \tag{21}$$

As equation (21) is linear in the time derivative of the state vector $\dot{\mathbf{x}}$ and the Jacobian matrix $\frac{\partial \mathbf{F}}{\partial \dot{\mathbf{x}}}$ proves to be non singular, a closed-form representation of the system dynamics can be obtained:

$$\dot{\mathbf{x}} = \mathbf{f}\left(\mathbf{x}, \mathbf{u}\right)\,. \tag{22}$$

3. HIGH-LEVEL MPC APPROACH

3.1 Mathematical formulation of Model Predictive Control

This subsection deals with the mathematical formulation of model predictive control schemes in general. Therefore, no assumptions regarding linear models are made. The equations presented in this section are based on the mathematical formulation of nonlinear model predictive control by Findeisen and Allgöwer [2002] adapted to discrete time-setting. The discrete-time system to be controlled is described by a nonlinear set of difference equations

$$\mathbf{x}_{k+1} = \mathbf{f}\left(\mathbf{x}_k, \mathbf{u}_k\right)\,, \tag{23}$$

where the index $k \in \mathbb{N}_0$ denotes the state or control input of the system at k^{th} sampling instant. Both the state vector $\mathbf{x}$ and the input vector $\mathbf{u}$ are constrained by:

$$\mathbf{u} \in \mathcal{U},\, \forall k\,, \tag{24}$$

$$\mathbf{x} \in \mathcal{X},\, \forall k\,. \tag{25}$$

In the simplest form the constraints $\mathcal{U}$ and $\mathcal{X}$ are given by

$$\mathcal{U} := \left\{\mathbf{u} \in \mathbb{R}^m \mid \mathbf{u}_{\min} \leq \mathbf{u} \leq \mathbf{u}_{\max}\right\}\,, \tag{26}$$

$$\mathcal{X} := \left\{\mathbf{x} \in \mathbb{R}^n \mid \mathbf{x}_{\min} \leq \mathbf{x} \leq \mathbf{x}_{\max}\right\}\,, \tag{27}$$

where m denotes the dimension of the input vector $\mathbf{u}$ and n denotes the dimension of the state vector $\mathbf{x}$. $\mathbf{u}_{\min}$, $\mathbf{u}_{\max}$ and $\mathbf{x}_{\min}$, $\mathbf{x}_{\max}$ are predefined constant vectors. The control law is represented by the discrete-time finite horizon open-loop optimal control problem (OCP) of finding an input sequence $\bar{\mathbf{u}}$ that minimises the quadratic cost functional $J\left(\cdot\right)$ such that:

$$\min_{\bar{\mathbf{u}}} J\left(\mathbf{x}_k, \bar{\mathbf{x}}, \bar{\mathbf{u}}; T_c, T_p\right)\,. \tag{28}$$

The cost functional is given by

$$\begin{aligned} J\left(\bar{\mathbf{x}}, \bar{\mathbf{u}}; T_c, T_p\right) = {} & \left(\bar{\mathbf{x}}_N - \mathbf{x}_N^*\right)^T \mathbf{P} \left(\bar{\mathbf{x}}_N - \mathbf{x}_N^*\right) \\ & + \sum_{j=0}^{N-1} \left[\left(\bar{\mathbf{x}}_j - \mathbf{x}_j^*\right)^T \mathbf{Q}_\mathbf{x} \left(\bar{\mathbf{x}}_j - \mathbf{x}_j^*\right)\right. \\ & \left. + \left(\bar{\mathbf{u}}_j - \mathbf{u}_j^*\right)^T \mathbf{Q}_\mathbf{u} \left(\bar{\mathbf{u}}_j - \mathbf{u}_j^*\right)\right] \end{aligned} \tag{29}$$

subject to

$$\bar{\mathbf{x}}_{j+1} = \mathbf{f}\left(\bar{\mathbf{x}}_j, \bar{\mathbf{u}}_j\right),\, \bar{\mathbf{x}}_0 = \mathbf{x}_k\,, \tag{30}$$

$$\bar{\mathbf{u}}_j = \begin{cases} \in \mathcal{U} & , N \leq M \\ \bar{\mathbf{u}}_M & , N > M \end{cases}\,, \tag{31}$$

$$\bar{\mathbf{x}}_j \in \mathcal{X}\,, \tag{32}$$

where the index $j \in \mathbb{N}_0$ denotes the internal state vector $\bar{\mathbf{x}}$ and the internal input vector $\bar{\mathbf{u}}$ at the j^{th} prediction instant for the k^{th} sampling instant. Only the first element $\bar{\mathbf{u}}_0$ is implemented. $N = T_p/\delta$ is the number of steps within the prediction horizon T_p and $M = T_c/\delta$ is number of steps within the control horizon T_c where δ is the prediction step size. The asterisk symbol denotes references for both state vector and input vector. The weighting matrices $\mathbf{Q}_\mathbf{x}$ and $\mathbf{Q}_\mathbf{u}$ penalise deviations from the reference for the state and input vectors respectively. $\mathbf{P}$ is the terminal weighting matrix for deviations of the state vector at the end of the prediction horizon. In the context of this paper, it is assumed that the terminal penalty matrix equals the weighting matrix for state deviations $\mathbf{Q}_\mathbf{x}$. The initial value of equation (30) $\mathbf{x}_k$ introduces state feedback to the MPC.

Table 1. Constraints for high-level linear MPC

Constraint subject to	Identifier	Unit	Constraint
Height above ground	$-z$	m	$[0, 4.0]$
Roll angle	ϕ	–	$[-\frac{\pi}{6}, \frac{\pi}{6}]$
Pitch angle	θ	–	$[-\frac{\pi}{6}, \frac{\pi}{6}]$
Vehicle attitude rates	p, q, r	rad/s	$[-\pi, \pi]$
Collective thrust	f_T	N	$[0, 14.0$ [1] $]$

3.2 Implementation

To obtain a linear prediction model, equation (21) is linearised at the setpoint for steady-state hovering:

$$\mathbf{x}_0 = (\mathbf{r}_0, 0, \ldots, 0, x_{L,0}, y_{L,0}, 0, 0) \,, \tag{33}$$

$$\mathbf{u}_0 = (\mathbf{0}, f_{T,0}) \,. \tag{34}$$

The setpoint of the position of the vehicle $\mathbf{r}_0$ is not relevant for the linearisation. The setpoint of the x-component and the y-component of the position of the load $(x_{L,0}, y_{L,0})$ is equivalent to the setpoint of the vehicles position in the xy-plane. The setpoint for the collective thrust $f_{T,0}$ equals the gravity force of the coupled system:

$$f_{T,0} = (m_F + m_L)\, g \,. \tag{35}$$

Whilst the reference for the input vector is constantly chosen identically to the input vector at the setpoint

$$\mathbf{u}^* = \mathbf{u}_0 \,, \tag{36}$$

the reference for the state vector depends on the flight manoeuvre to be performed. The later yields a time-variant control law for the MPC.

The constraints for the high-level linear MPC scheme are listed in table 1. The constraint in the z-position is chosen with regard to the real flight experiment. Both the limitation of the vehicle's roll and pitch angle and the limitation of the maximum attitude rates prevents potentially dangerous flight manoeuvres. The weighting matrices are given by:

$$\mathbf{Q_x} = \operatorname{diag}(0.1, 0.1, 1, 10^{-6}, \ldots, 10^{-6}, 1, 1, 10^{-6}, 10^{-6}) \,, \tag{37}$$

$$\mathbf{Q_u} = \operatorname{diag}(10^{-2}, \ldots, 10^{-2}) \,. \tag{38}$$

The term $\operatorname{diag}(\cdot)$ refers to a matrix with the vector denoted as a parameter forming the principal diagonal of the matrix. All the other entries equal zero. Deviations in the position of the load are penalised ten times stronger than deviations in the position of the vehicle. This refers to potential real world applications where it might be desired to track the load precisely. Further controller parameters are listed in table 2.

[1] Measured maximum for the DJI F330 with 3s lithium polymer accumulator

Table 2. High-level controller parameters

Parameter	Identifier	Unit	Value
Update rate	$\frac{1}{T_s}$	Hz	80.000
Prediction horizon	T_p	s	5.0000
Prediction step size	δ	s	0.1000
Control horizon	T_c	s	5.0000

Table 3. Physical parameters of the system

Parameter	Identifier	Unit	Value
Mass of the vehicle	m_F	kg	0.9300
Number of rotors	N_R	–	4
Mass of the load	m_L	kg	0.2000
Cable length	l	m	1.0000
Cross-section area of the load	A_L	m^2	0.0142
Drag coefficient of the load	$C_{D,L}$	–	1.2000
Gravitational acceleration	g	m/s^2	0.9810
Density of the air	ρ	kg/m^2	1.1840

4. SIMULATION

4.1 Simulation Environment

The simulation is set up using MATLAB and Simulink. The nonlinear dynamics given by equation (22) are used for the simulation model. The physical parameters for both the linear prediction model and the nonlinear simulation model are listed in table 3. The ACADO Toolkit is integrated to solve the OCP emerging from the MPC approach (cf. Houska et al. [2011]).

A linear-quadratic regulator (LQR) control approach is implemented to compare the performance of the MPC scheme to a more classical optimal control strategy. The constant feedback matrix is obtained by executing the MATLAB built-in `lqr()` command with the same linear model state-space representation as used for the MPC prediction model. Hence, no integral action is superinduced. The weighting matrices are chosen identically to the ones applied to the MPC.

4.2 Simulation Results

The simulation of an exemplary test case of tracking a predefined trajectory is demonstrated within this paper. The reference state vector $\mathbf{x}^*$ contains non-zero elements only where the trajectory of the vehicle and the load is influenced directly. These elements are $\mathbf{r}^* = (x^*, y^*, z^*)$. The reference for the load's position in the x and y-components is equal to the reference for the vehicle's position. The reference trajectory is a figure-eight curve in the $\mathbf{x}_\mathcal{I}\mathbf{y}_\mathcal{I}$-plane. The values in meters are given by:

$$\mathbf{r}^* = (2\sin(\omega t)\,, 2\sin(\omega t)\cos(\omega t)\,, -1.5) \,. \tag{39}$$

The frequency is ramped up from zero to $\omega = 0.4\,\mathrm{rad/s}$ within the first four seconds of the simulation. The predefined reference states spanning the prediction horizon are

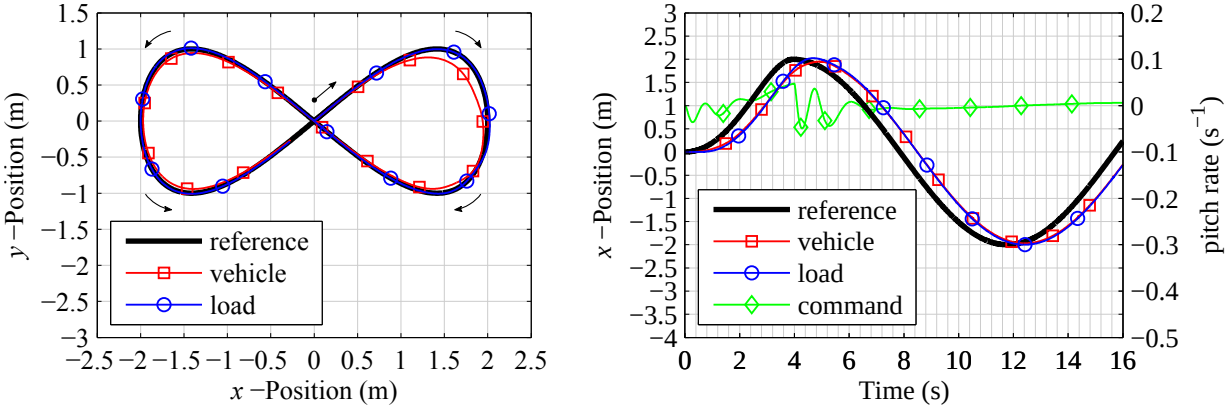

(a) Ground track (LQR)

(b) x-Position over the course of time (LQR)

Fig. 2. Simulation, LQR: Figure-eight curve tracking

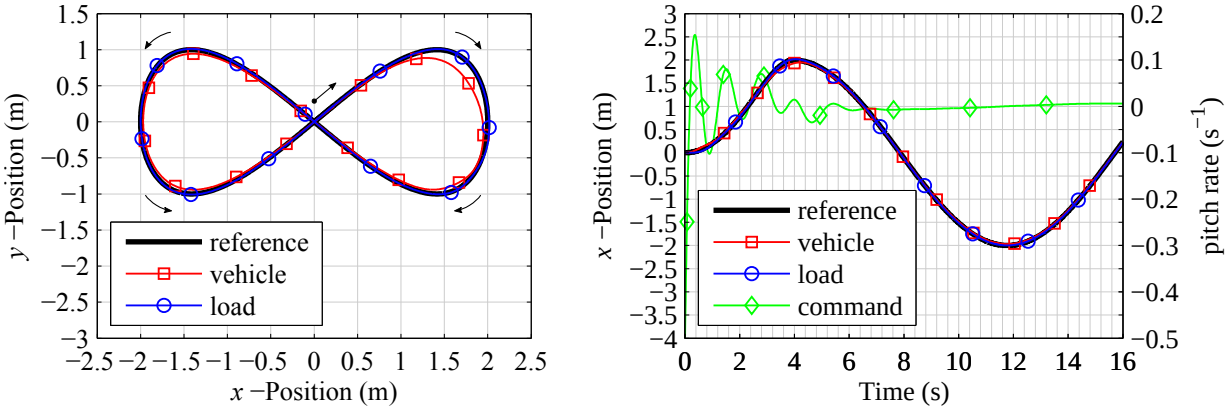

(a) Ground track (MPC)

(b) x-Position over the course of time (MPC)

Fig. 3. Simulation, MPC: Figure-eight curve tracking

fed to the MPC at each controller update. The state of the simulation model is fed back to the controller without any additional noise.

Fig. 2 shows the ground track and the x-position over the course of time for the system using the LQR control approach. The corresponding plots for the system subject to the MPC approach are displayed in Fig. 3. The impact of accelerating from a state of rest at the beginning of the simulation can be seen in the asymmetric flight path depicted in Subfig. 2a and 3a respectively. Because of the higher weightings for deviations in the load's position, both control approaches aim to minimise the overshoot of the load by moving the vehicle slightly inside the reference trajectory. For the system subject to the MPC approach, the mean deviation for the x-position of the vehicle equals 34.6 mm, whereas the mean deviation for the x-position of the load equals 10.3 mm. The system using the LQR control approach lags in time by approximately 0.8 seconds (cf. Subfig. 2b). As can be seen in Subfig. 3b, the MPC commands a more aggressive pitch rate sequence, resulting in a higher control effort compared to the system subject to the LQR. Although not being hit within the test case presented, the ability to take constraints into account gives preference to the MPC approach for real flight applications.

5. FLIGHT TEST

5.1 Flight Test Environment

The ARCAA Indoor Flying Laboratory is set up to design and verify control algorithms for UAVs. The global position and attitude are provided by an infrared motion capture system via Ethernet. The velocity of the vehicle and the load is obtained by numerical differentiation. A nonlinear state estimator as presented in Lupashin et al. [2014] is applied in order to both reject corrupted measurements and account for system latency. The user code runs on a desktop computer. The commands are transmitted wirelessly to the vehicle. The core component is a software module which is solely implemented in Simulink. Onboard the vehicle, a μ-controller decodes the radio signals and converts the serial input to a pulse-width modulated output, which is fed into a low-level PID controller. The physical parameters of the real system are identical with those of the simulated system listed in table 3. For the flight experiment, an integral gain acting in parallel to the MPC penalises deviations in the z-direction in order to compensate for thrust miscalibration.

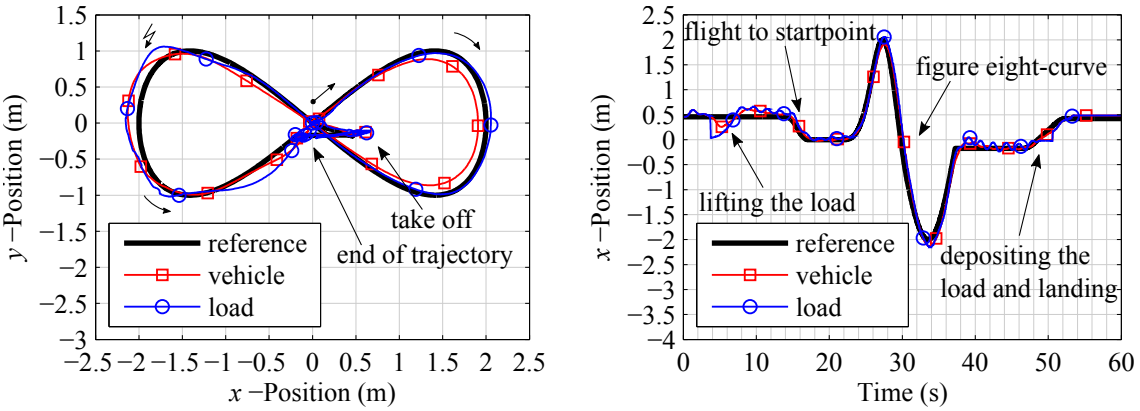

(a) Ground track (flight test)

(b) x-Position over the course of time (flight test)

Fig. 4. Flight Test: Figure-eight curve tracking with flight segment labeling

5.2 Flight Test Results

A test flight using the same reference trajectory as defined in subsection 4.2 is presented here. The whole flight from take off to landing is shown in Fig. 6. The data is captured by infrared cameras at a sampling rate of 200 Hz. A moving average low-pass filter is applied over ten consecutive measuring points. As the weighting matrices are chosen equal to those used in the simulation, the controller aims at keeping the position of the load aligned with the reference rather than the position of the vehicle. Similar to simulation, the impact of the stronger penalisation for deviations in the load's position can be seen in Subfig. 4a on the first leg of the figure-eight curve (corresponding to positive values for x). The overshooting of the load's x-position is kept below 60 mm. On the second leg the trajectory reaches the border of the camera coverage. The spurious measurement results in a less accurate tracking performance. The system lags in time by under half a second, whereby the load's position lags in time more than the vehicle's position (cf. Subfig. 4b). The authors ascribe this fact to undervaluing the aerodynamic drag force of the load in the prediction model (cf. table 3). Nonetheless, accurate four-dimensional tracking performance of the MPC approach shown in simulation is verified by the flight test results.

6. CONCLUSION

In this work, a mathematical model for the coupled system dynamics of a multirotor UAV with heavy slung load has been derived. Based on this model, a Model Predictive Control scheme has been set up. Simulation results for the test case of tracking a figure-eight curve have been discussed. For the given implementation, the MPC scheme's superior ability for tracking a predefined, time-dependent reference in comparison to a system using an LQR control approach has been shown. The feasibility of the predictive control approach has been demonstrated in flight tests.

For outdoor use of a multirotor UAV with heavy slung load implementing an MPC scheme as presented within this paper, one needs to become independent from using a motion capture system. A setup for visual load detection using an onboard camera is presented by Zürn et al. [2016]. The feasibility of running a specially tailored MPC on an onboard computer of a small UAV is demonstrated by Joos and Fichter [2011].

REFERENCES

Findeisen, R. and Allgöwer, F. (2002). An introduction to nonlinear model predictive control. In *21st Benelux Meeting on Systems and Control, Veldhoven*.

Hehn, M. and D'Andrea, R. (2011). A flying inverted pendulum. In *IEEE International Conference on Robotics and Automation (ICRA)*, 763–770.

Houska, B., Ferreau, H.J., and Diehl, M. (2011). Acado toolkit – an open-source framework for automatic control and dynamic optimization. *Optimal Control Applications and Methods*, 32(3), 298–312.

Joos, A. and Fichter, W. (2011). Parallel implementation of constrained nonlinear model predictive controller for an fpga-based onboard flight computer. *Advances in Aerospace Guidance, Navigation and Control*, 273–286.

Lupashin, S., Hehn, M., Mueller, M.W., Schoellig, A.P., Sherback, M., and D'Andrea, R. (2014). A platform for aerial robotics research and demonstration: The flying machine arena. *Mechatronics*.

Oktay, T. and Sultan, C. (2013). Modeling and control of a helicopter slung-load system. *Aerospace Science and Technology*.

Omar, H. (2009). New fuzzy-based anti-swing controller for helicopter slung-load system near hover. In *IEEE International Symposium on Computational Intelligence in Robotics and Automation (CIRA)*, 474–479.

Sreenath, K., Lee, T., and Kumar, V. (2013). Geometric control and differential flatness of a quadrotor uav with a cable-suspended load. In *IEEE 52nd Annual Conference on Decision and Control (CDC)*, 2269–2274.

Trachte, J., Gonzalez, F., and Mcfadyen, A. (2014). Nonlinear model predictive control for a multi-rotor with heavy slung load. In *International Conference on Unmanned Aircraft Systems (ICUAS)*, 1105–1110.

Zürn, M., McFadyen, A., Notter, S., Heckmann, A., Morton, K., and Gonzalez, L.F. (2016). Mpc controlled multirotor with suspended slung load: System architecture and visual load detection. In *2016 IEEE Aerospace Conference*. Yellowstone Conference Center, Big Sky, Montana.